

# Scaling Properties of Fluctuations in Human Electroencephalogram

**Rudolph C. Hwa**

Institute of Theoretical Science and  
Department of Physics  
University of Oregon, Eugene, OR 97403-5203

**Thomas C. Ferree**

Dynamic Neuroimaging Laboratory  
Department of Radiology  
University of California San Francisco  
San Francisco, CA 94143-0628

The fluctuation properties of the human electroencephalogram (EEG) time series are studied using detrended fluctuation analysis. For nearly all 128 channels in each of 28 subjects studied, it is found that the standard deviation of the fluctuations exhibits scaling behaviors in two regions. Topographical plots of the scaling exponents reveal the spatial structure of the nonlinear electrical activities recorded on the scalp. Moment analyses are performed to summarize the global variability across channels. The correlation between the two scaling exponents in each channel is also examined. Two global measures are found that succinctly characterize the overall properties of the fluctuation behaviors of the brain dynamics for each subject. Together they distinguish the stroke subjects from the normal ones with 90% accuracy, suggesting the possibility that this analysis could lead to an effective diagnostic tool.

Submitted to *Physical Review E*

## I. INTRODUCTION

The scalp electroencephalogram (EEG) provides a wealth of information about human brain dynam-

ics. The complex nature of the brain results in a high degree of fluctuations in both the spatial and temporal aspects of the EEG signals. To extract the salient properties from the data is the primary objective of any method of analysis. We present in this paper a novel combination of techniques that explores the scaling behavior of the temporal fluctuations, then uses moment analysis to summarize the spatial variability across many electrode channels.

The most common methods of EEG time series analyses are event-related time ensemble averaging and Fourier decomposition, both of which are based implicitly on assumptions of linearity [1,2]. Since the physiological mechanisms underlying the scalp EEG are generally nonlinear, they can generate fluctuations that are not best described by linear decomposition. Moreover, the resting EEG always displays a broad-banded power spectrum, so in Fourier analysis one must arbitrarily define frequency bands ( $\delta, \theta, \alpha, \dots$ ) which may not actually delineate different dynamical mechanisms unless tailored to each subject functionally. Wavelet analyses have also been applied to examine EEG time series [3], but at a sacrifice of the ability to describe long-range temporal correlations. To quantify the nonlinear behavior of the EEG, chaos analyses have been applied [4–6], but typically require a long period of time to compute attractor properties for a single time series. Moreover, chaos-based approaches assume the existence of low-dimensional attractors, and this is probably not a valid assumption for EEG dynamics generally. In this paper, we employ a method that analyzes the temporal fluctuations in the resting EEG over a relatively short period of time ( $\sim 10$ s), and avoids the assumptions of linearity and low-dimensional chaos. We demonstrate the existence of scaling behavior of the fluctuations in nearly all channels and all subjects studied.

The EEG voltage time series analyzed here were collected from 128 electrodes distributed uniformly over the scalp, relative to a reference electrode located at the top of the head. An open challenge is how best to analyze the large amount of data coming from this many channels. We aim to find what is universal among all channels as well as what varies among them. The former is obviously important by virtue of its universality for a given subject; how that universal quantity varies from subject to subject is clearly interesting. What varies from channel to channel is perhaps even more interesting, since it has implications for describing focal features which may have functional or clinical relevance. Our procedure is to focus initially on one channel at a time, and determine a few parameters (scaling exponents) that effectively summarize the temporal fluctuations. The second phase of our procedure is to describe the global behavior of all channels and to arrive at two numbers that summarize the variability of the scaling exponents across the entire scalp surface. This intentional effort toward data reduction necessarily trades detail for succinctness, but such reduction is exactly what is needed to allow easy discrimination between brain states or between subgroups.

The emphasis in this paper is on the method of analysis more than its application. We motivate and develop the analyses which extract the power-law behaviors in the EEG. Since our approach is unconventional, it may be more persuasive if we can provide some preliminary evidence of its utility. To this end, we apply the analysis to two subject groups: normal and those with acute ischemic stroke. We find that our two-parameter description for each subject effectively separates the two groups. This justifies *a posteriori* our approach, although it will require a body of future work to understand fully the dynam-

ical origins of these scaling laws.

## II. DETRENDED FLUCTUATION ANALYSIS

The specific method we use in the first phase is detrended fluctuation analysis (DFA). This analysis is not new. It was proposed for the investigation of correlation properties in DNA nucleotides [7] and extended to heartbeat time series [8]. It has been applied to EEG only once to our knowledge [9], but with somewhat different emphases than those presented here.

There is, however, an important difference between how we use DFA here, and how it has been applied to, say, the heartbeat time series [8]. Heartbeat information is the interbeat intervals that are discrete. As developed in [8], the fluctuations of the intervals from their long-time average are treated as the steps taken by a random walker, and the partial integral of the steps becomes the random-walk time series, to which the DFA is applied. The resulting scaling behavior can then be related to the nature of the correlations in the time series and an interpretation be given to the scaling exponents. As an example of that interpretation one can note that the standard deviation of the usual unbounded random-walk time series increases as the square root of the number of steps; hence, the scaling exponent is 0.5. For that interpretation to be effective the time series must be long. The heartbeat problem treated in [8] involves very long time series, up to 24 hours. Our problem is very different. The EEG time series is continuous and bounded, and the data segments we analyze for most clinical applications are relatively short ( $\sim 10$ s). We therefore apply DFA to it directly without integration. As a consequence, we lose the availability of any simple way to interpret our results, such as in the framework of the random-walk

problem. Nevertheless, our approach yields meaningful description of the fluctuations when taken in the context of global characterization. Further comments to clarify our approach will be made at the end of the next section.

To be definitive, let an EEG time series be denoted by  $y(t)$ , where  $t$  is discrete time ranging from 1 to  $T$ . Divide the entire range of  $t$  to be investigated into  $B$  equal windows, discarding any remainder, so that each window has  $k = \text{floor}(T/B)$  time points. Within each window, labeled  $b$  ( $b = 1, \dots, B$ ), perform a least-square fit of  $y(t)$  by a straight line,  $\bar{y}_b(t)$ , i.e.,  $\bar{y}_b(t) = \text{Linear-fit}[y(t)]$  for  $(b-1)k < t \leq bk$ . That is the semi-local trend for the  $b$ th window. Define  $F_b^2(k)$  to be the variance of the fluctuation  $y(t)$  from  $\bar{y}_b(t)$  in the  $b$ th window, i.e.,

$$F_b^2(k) = \frac{1}{k} \sum_{t=(b-1)k+1}^{bk} [y(t) - \bar{y}_b(t)]^2 \quad (1)$$

It is a measure of the semi-locally detrended fluctuation in window  $b$ . The average of  $F_b^2(k)$  over all windows is

$$F^2(k) = \frac{1}{B} \sum_{b=1}^B F_b^2(k). \quad (2)$$

$F(k)$  is then the RMS fluctuation from the semi-local trends in  $B$  windows each having  $k$  time points.

The study of the dependence of  $F(k)$  on the window size  $k$  is the essence of DFA [7,8]. If it is a power-law behavior

$$F(k) \propto k^\alpha, \quad (3)$$

then the scaling exponent  $\alpha$  is an indicator of the nature of the fluctuations in EEG. Since DFA considers only the fluctuations from the semi-local linear trends, it is insensitive to spurious correlations introduced by slowly-varying external trends. This is a practical advantage since EEG acquisition systems

often suffer from very slow ( $< 0.1$  Hz) drifts associated with gradual changes in the quality of electrode contact to the skin, for example. The analysis also liberates our result from the dependence on the overall magnitude of the voltage  $y(t)$  recorded by each probe, which is an advantage since overall signal amplitude can vary across subjects, presumably due to differences in skull conductivity and other factors.

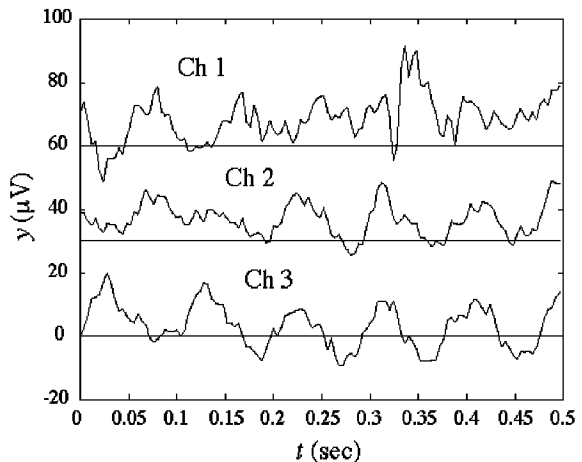


FIG. 1. A sample of EEG time series in three channels. The vertical scales of Ch. 1 and Ch. 2 are shifted upward by 60 and 30  $\mu\text{V}$ , respectively.

Resting EEG data were collected [10] for 28 subjects using a 128-channel commercial EEG system (Electrical Geodesics, Inc.), with scalp-electrode impedances ranging from 10 to 40  $k\Omega$ . The data were hardware filtered between 0.1 and 100 Hz, then digitized at 250 points/sec. After acquisition,  $T \approx 10$  s lengths of simultaneous time series in all channels were chosen, free of artifacts such as eye blink and head movements. At each time point, the average across all electrodes was subtracted, to remove approximately the effect of the reference electrode [2]. We investigate the range of  $k$  from 3 to 500 in approximately equal steps of  $\ln k$ . We have verified that computing  $F(k)$  for all  $k$  from 3 to 500 sim-

ply interpolates these value and does not affect the computed scaling exponents  $\alpha_i$ .

In Fig.1 we show three typical time series  $y(t)$  in three widely separated channels for subject A, labeled 1-3, for brevity. While it is clear that both channels 2 and 3 have substantial 10 Hz oscillations after 0.2s, it is much less apparent that there exist any scaling behaviors in all three channels. The corresponding values of  $F(k)$  are shown in the log-log plot in Fig. 2.

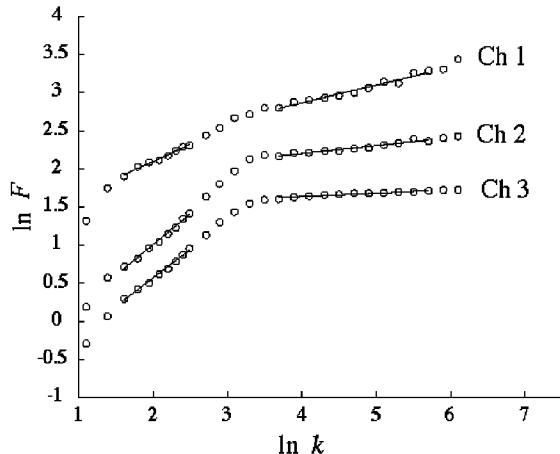


FIG. 2.  $F(k)$  versus  $k$  for the three channels in Fig. 1. The vertical scales of Ch. 1 and Ch. 2 are shifted upwards by 1.0 and 0.5 units, respectively.

Evidently, the striking feature is that there are two scaling regions with a discernible bend when the two slopes in the two regions are distinctly different. With rare exceptions this feature is found in all channels for all subjects. Admittedly, the extents of the scaling regions are not wide, so the behavior does not meet the qualification for scaling in large critical systems or in fractal geometrical objects. However, since the behavior is so universal across channels and subjects, and since the temporal scales involved are physiologically relevant, this scaling behavior is a feature of EEG that conveys a unifying property of

the dynamics across temporal scales and warrants further investigation.

### III. SCALING AND NONSCALING PROPERTIES

To quantify the scaling exponents, we perform a linear fit in Region I for  $1 < \ln k < 2.5$  and denote the slope by  $\alpha_1$ , and similarly in Region II for  $3.5 < \ln k < 5.75$  with slope denoted by  $\alpha_2$ . Visual inspection for each of the 28 subjects verifies that fitting this way does a remarkably good job of characterizing the slopes in the two regions. Knowing the two straight lines in each channel allows us to determine the location of their intercept,  $\ln \kappa$ , which gives a good approximation for the position of the bend in  $\ln k$ . We find that, whereas  $\alpha_1$  and  $\alpha_2$  can fluctuate widely from channel to channel,  $\kappa$  is limited to a narrow range in most subjects. The average value of  $\ln \kappa$  for each subject ranges from 2.6 to 3.6, with a grand average across subjects to be approximately 3.1. It should, however, be noted that when  $\alpha_1$  and  $\alpha_2$  are nearly the same, as is the case for Ch. 1 in Fig. 2, the determination of  $\kappa$  by the intersection of the two straight lines is not reliable. Nevertheless, it is visually clear that the bend occurs in the vicinity of  $\ln \kappa = 3.1$ .

Since scaling behavior means that the system examined has no intrinsic scale, scale noninvariance at  $\kappa$  implies that  $\kappa$  is related to a characteristic time scale in the data. From Fig. 1 one indeed sees roughly periodic oscillations in Ch. 2 and 3. It is at this point that a contact can be made with the usual Fourier analysis. Although our analysis focuses on scale invariant quantities, i.e., the dimensionless scaling exponents, it is worth digressing momentarily to establish this contact. To do this, we loosely associate the time scale  $\kappa$  with the period

of a sine wave with frequency  $f$ . If the data acquisition rate is denoted by  $r$ , then the frequency  $f$  corresponding to  $\kappa$  is

$$f = \frac{r}{\kappa}. \quad (4)$$

For our data acquisition we have  $r = 250$  points/sec. For the across-subject average of  $\ln \kappa = 3.1$ , we get from Eq. (4)  $f = 11.3$  Hz. That is in the middle of the traditional  $\alpha$  (8-13 Hz) EEG frequency band. Thus the dominant periodic oscillation apparent in Fig. 1 does reveal itself in the study of the scaling behavior.

Now that we have noted the relationship between the bend in  $F(k)$  and the dominant frequency of sinusoidal oscillation in the data, a word of caution is in order. One may be tempted to think that if, instead of considering the fluctuations from the linear semi-local trends  $\bar{y}_b(t)$ , one studies the fluctuations from periodic oscillations, then the bend might disappear and the two scaling regions might be joined to become one. Even if that were true, such a procedure should not be used for two reasons. First, not all channels exhibit obvious oscillatory behaviors with definite frequencies. Whatever detrending one chooses should be universally applied to all channels in order to avoid introducing discrepancies across the channels due to external intervention. Second, to determine the frequency of the oscillatory trend requires a Fourier analysis, which is precisely what our approach attempts to circumvent. To decide on a sinusoidal wave of a particular frequency as reference for detrending involves arbitrariness and is unlikely to lead to any simplification in the global picture. The simplest and least biased approach is to use the semi-local linear trends, as we have done. If one's interest is in the sinusoidal frequency content of the EEG time series, then Fourier analysis is direct. Alternatively, if one's interest is in the fluctu-

ations generally and their relationships *across* time scales, then DFA allows a more succinct parametrization. Hereafter, frequency plays no essential role in this paper.

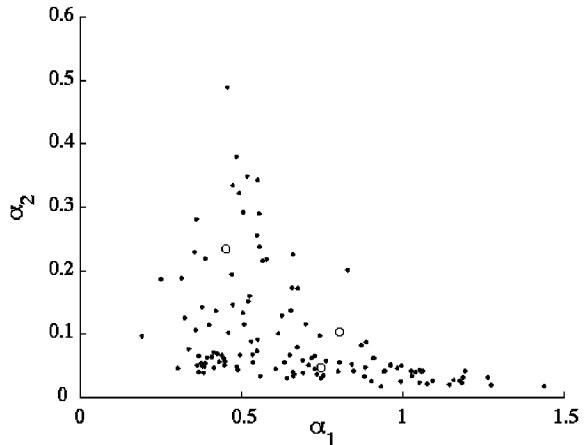


FIG. 3. Scatter plot of  $\alpha_2$  versus  $\alpha_1$  for subject A. The three channels exhibited in Figs. 1 and 2 are shown as circles.

For each subject we have 128 pairs of values of  $(\alpha_1, \alpha_2)$ , which summarize the temporal fluctuations in terms of scaling exponents. In Fig. 3, we exhibit by scatter plot the values of  $\alpha_1$  and  $\alpha_2$  of all channels for subject A. The three points marked with circles correspond to the channels shown in Fig. 2. Overall, for subject A, the scaling exponents are in the ranges:  $0.19 < \alpha_1 < 1.44$  and  $0.018 < \alpha_2 < 0.489$ . Whereas  $\alpha_1$  is widely distributed,  $\alpha_2$  is sharply peaked at 0.1 and has a long tail. Region I corresponds to fluctuations over short time scales, Region II over long time scales, with  $\kappa$  giving a quantitative demarcation between the two. In most channels we find  $\alpha_1 > \alpha_2$ , although there are a few where  $\alpha_1 \approx \alpha_2$ . The scatter plots of all other subjects are similar in general features to the one shown in Fig. 3, but vary in detail from subject to subject. It is impractical to show them all in this paper. Evidently, it is desirable to find a way

to quantify succinctly these 128 pairs of numbers so that one can effectively compare the results across subjects.

Since our application of DFA differs from that of previous authors, in that we do not integrate the EEG time series, some comments are in order on the theoretical significance of the  $\alpha_i$  values obtained here. Since the EEG time series is bounded, one should expect that, as  $k \rightarrow \infty$ ,  $F(k)$  becomes a constant, and that the asymptotic slope  $\alpha_\infty$  becomes zero. Since we find that usually  $\alpha_2 < \alpha_1$ , one may be tempted to regard the changes of slopes in Fig. 2 as preludes toward the asymptotic behavior just noted, and to dismiss the significance of the two scaling regions. There are several arguments against such a view. Firstly, the bend separating the two scaling regions occurs at a physiologically meaningful time scale and usually abruptly. In contrast, the bend toward constancy due to the asymptotic requirement can occur gradually over any range of  $k$  and has no obvious physiological significance beyond the fact that the EEG is bounded. Secondly, most of the values of  $\alpha_2$  are far from zero, and in some cases  $\alpha_1 \approx \alpha_2$  or  $\alpha_1 < \alpha_2$ . They fluctuate widely across channels, as is evident from the scatter plot in Fig. 3. Indeed, we give appropriate weight to the large values of  $\alpha_2$  in the moment analysis below. The fact that in some channels  $\alpha_2 \approx \alpha_1$  implies that there is little bending between Regions I and II and that the asymptotic behavior  $\alpha \rightarrow 0$  as  $k \rightarrow \infty$  has no effect in the data analyzed. Thirdly, knowing the asymptotic behavior does not imply that there is no valuable information contained in the non-asymptotic behavior. To extract such information is especially important when there are clinical reasons for the impracticality of obtaining very long time series, in which the asymptotic limit may become evident. Finally, although the individual values of  $\alpha_1$

and  $\alpha_2$  cannot be given a simple interpretation, as one could with the scaling exponents of long random-walk time series, the  $\alpha_i$ 's should be regarded as the bricks in the building of a global structure that can characterize the general brain state of a subject.

#### IV. MOMENTS OF THE SCALING EXPONENTS

A scatter plot such as Fig. 3 reveals very well how the  $\alpha_i$  exponents of all the channels are related to one another. However, it shows nothing about the locations of the channels on the scalp. To show that, we can make topographical plots of  $\alpha_1$  and  $\alpha_2$  separately, as in Fig. 4.

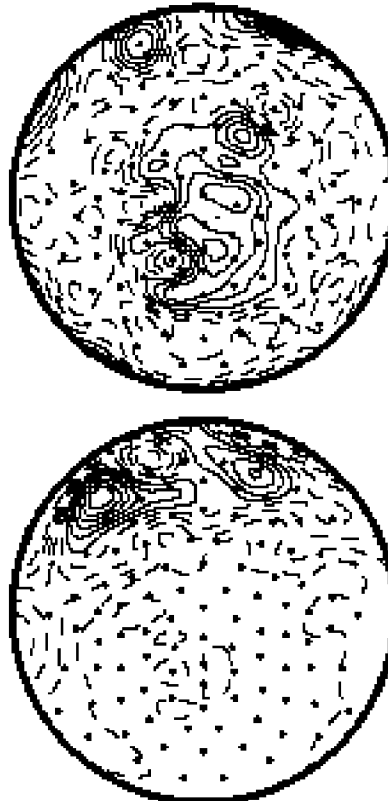


FIG. 4. Topographical plots of  $\alpha_1$  (top) and  $\alpha_2$  (bottom). In each figure, ten contour lines are drawn within the data range: solid lines above the mean, dotted lines below.

It is seen that they each vary systematically over the scalp, and that the range of their variability is large compared to the errors in their calculation. Such plots may be useful for attempting to localize focal features, e.g., associated with particular brain functions and/or pathologies. However, there are cases in which EEG changes are known to be not spatially localized with the site of pathology. Ischemic stroke is one such example [11]. It is therefore of great interest to develop few-parameter descriptions of global brain state, to facilitate comparisons across subjects, and to quantify brain state without necessarily presuming spatial localization. To this end, we develop here a novel approach for analyzing the variability of the scaling exponents with the aim of getting global measures.

We propose to consider the moments of the scaling exponents. In general, if we have  $N$  numbers,  $z_j, j = 1, \dots, N$ , we can calculate the moments

$$G_q = \frac{1}{N} \sum_{j=1}^N z_j^q, \quad (5)$$

where  $q$  is a positive integer [12]. The information contained in the first  $N$  moments (i.e.,  $q = 1, \dots, N$ ) is enough to reproduce all the  $z_j$  by inversion. However, we may be interested in only a few of the  $G_q$  with lower order  $q$ , each of which contains some information of all the  $z_j$ . In our present problem we have  $N = 128$ , and we shall consider the first ten orders,  $1 \leq q \leq 10$ . That is a significant step in data reduction, a process worth investigating.

Before calculating the moments of  $\alpha_i$ , let us see how those values are distributed. Let  $x$  be either  $\alpha_1$  or  $\alpha_2$ . Since no value of  $\alpha_i$  has been found to exceed 1.5 in the subjects we have examined, we consider the interval  $0 \leq x \leq 1.5$ . Divide that interval into  $M$  equal cells, which for definiteness we take to be  $M = 150$  here. Let the cells be labeled by  $m = 1, \dots, M$ , each having the size  $\delta x = 1.5/M$ . Denote

the number of channels whose  $x$  values are in the  $m$ th cell by  $n_m$ . Define

$$P_m = n_m / N. \quad (6)$$

It is the fraction of channels whose  $x$  values are in the range  $(m-1)\delta x \leq x < m\delta x$ . By definition, we have  $\sum_{m=1}^M P_m = 1$ . In Fig.5 we show as an illustration the two graphs of  $P_m$  for subject A. The two graphs correspond to  $\alpha_1$  and  $\alpha_2$ , and are, in essence, the projections of the scatter plot in Fig.3 onto the  $\alpha_1$  and  $\alpha_2$  axes. From Fig.5 we see that  $\alpha_1$  is widely distributed, while  $\alpha_2$  is not (in absolute values), but has a long tail relative to its mean.  $G_1$  gives the average, and  $G_2$  is related to the width.

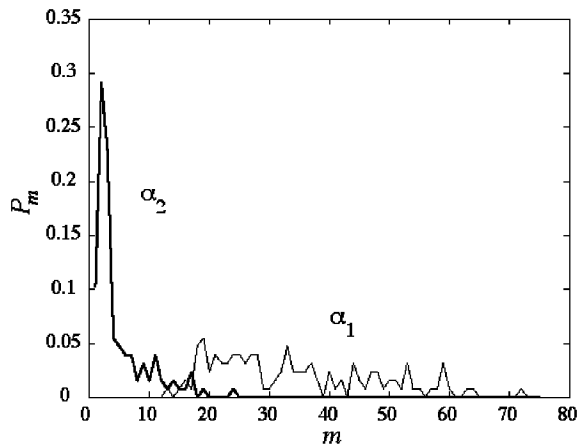


FIG. 5. The distributions  $P_m$  for  $\alpha_1$  and  $\alpha_2$ . The window size in  $\alpha$  for this plot is 0.02.

Since the variance and other moments typically increase with the mean of a distribution, the fluctuation of  $m$  in  $P_m$  is best measured relative to its mean. Let us therefore consider the normalized moments [13]

$$\begin{aligned} M_q^{(i)} &= G_q^{(i)} / \left(G_1^{(i)}\right)^q \\ &= \frac{\sum_{m=1}^M m^q P_m^{(i)}}{\left(\sum_{m=1}^M m P_m^{(i)}\right)^q}, \end{aligned} \quad (7)$$

where  $i = 1$  or  $2$ . Since these moments are averages of  $(m/\bar{m})^q$ , where  $\bar{m}$  is the average- $m$ , they are not very sensitive to  $\bar{m}$  itself. They contain the essence of the fluctuation properties of  $\alpha_{1,2}$  in all channels. In terms of the scaling exponents explicitly, let us use  $\alpha_i(j)$  to denote the value of  $\alpha_i$  for channel  $j$  so that Eq.(7) may be rewritten as

$$M_q^{(i)} = \frac{1}{N} \sum_{j=1}^N \alpha_i(j)^q \bigg/ \left( \frac{1}{N} \sum_{j=1}^N \alpha_i(j) \right)^q. \quad (8)$$

In principle, it is possible to examine also the moments for  $q < 0$ , which would reveal the properties of  $P_m$  at low values of  $m$ . However, the accuracy of our data is not too reliable for low- $k$  analysis, since the 60 Hz noise due to ambient electric and magnetic fields has not been cleanly filtered out, and the sampling rate  $r = 250$  Hz does not allow meaningful scaling analysis for shorter time scales. In this paper, therefore, we restrict our study to only the positive  $q$  values. For high  $q$ , the large  $m/\bar{m}$  parts of  $P_m^{(1,2)}$  dominate  $M_q^{(1,2)}$ .

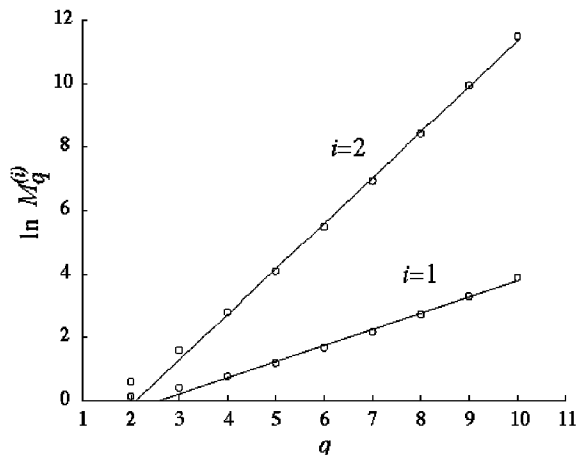


FIG. 6. The  $q$  dependence of  $\ln M_q^{(i)}$  for subject A. The straight lines are linear fits of the points for  $q \geq 5$ .

In Fig.6 the  $q$ -dependences of  $\ln M_q^{(1,2)}$  are shown for the distributions exhibited in Fig.5 for  $2 \leq q \leq 10$ . They are approximately linear except for the

low values of  $q$ . The same type of dependencies on  $q$  are found for all subjects. In Fig.6 we show two straight lines that can fit very well the nearly linear behaviors of  $\ln M_q^{(i)}$  versus  $q$  for  $q \geq 5$ . Thus for large  $q$  we have

$$M_q^{(i)} \propto \exp(\mu_i q), \quad q \geq 5. \quad (9)$$

The linear extrapolations of the lines to lower values of  $q$  show the degree of deviation of the the calculated values of  $\ln M_q^{(1,2)}$  from linearity. Since  $\ln M_q^{(1)}$  and  $\ln M_q^{(2)}$  behave so similarly in their departures from their linear dependencies on  $q$ , we plot  $\ln M_q^{(2)}$  versus  $\ln M_q^{(1)}$  in order to exhibit their direct relationship without explicit dependence on  $q$ . We find that they are linearly related over a wider range of values. This linearity is found to be true for all subjects. The plots for three of them are illustrated in Fig.7, where the straight lines are the linear fits.

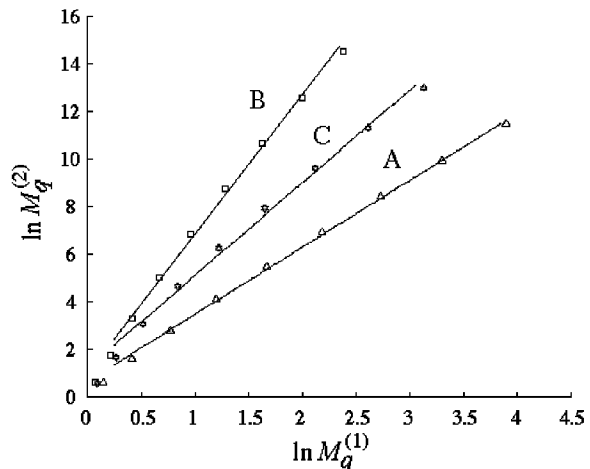


FIG. 7. A log-log plot of  $M_q^{(2)}$  versus  $M_q^{(1)}$  for three subjects A, B, and C. The solid lines have the slopes given by Eq. (10).

Thus the implication is that there exists a universal power-law behavior

$$M_q^{(2)} \propto \left( M_q^{(1)} \right)^\eta \quad (10)$$

valid for all subjects examined. From Eqs.(9) and

(10) we obtain

$$\eta = \mu_2/\mu_1, \quad (11)$$

but now  $\eta$  is meaningful for all  $q$  (except for the lowest points) and in that sense independent of  $q$ . Thus we have discovered a global measure  $\eta$  that characterizes all  $\alpha_i$  values of a subject, and varies from subject to subject. We postpone the display of the  $\eta$  values for all subjects until later.

To understand the exponential behavior in Eq.(9), we note that  $G_q$  is dominated by large  $z_j$  when  $q$  is large, as is self-evident in Eq.(5). For asymptotically large  $q$ , we have  $G_q \propto \exp(q \ln z_{\max})$ , where  $z_{\max} = \max\{z_j\}$ . For intermediate  $q$ , all large values of  $z_j$  can make important contributions, and the exponential dependence on  $q$  can still prevail. The denominator in Eq.(7) is  $G_1^q = \bar{z}^q = \exp(q \ln \bar{z})$ , where  $\bar{z}$  is the average of  $z_j$ , so it is also exponential for any  $q$ . It is therefore clear that Eq.(9) follows, and that  $\mu_i$  depends on all  $z_j$  with more weight on the large  $z_j$  values. The power-law behavior of Eq.(10) implies that the exponent  $\eta$  is independent of  $q$  and that all  $\alpha_i$  values are relevant contributors to the universal behavior. This is an important point worth emphasizing: the independence of  $\eta$  on  $q$  implies that the whole spectra of  $\alpha_1$  and  $\alpha_2$  are summarized by the one index  $\eta$ . The fact that  $\eta$  varies from subject to subject is a consequence of the variability of all 128 pairs of  $(\alpha_1, \alpha_2)$  across the subjects, and offers the possibility that  $\eta$  can be used as a discriminating representation of the brain state.

## V. CORRELATIONS OF THE SCALING EXPONENTS

The analysis in the preceding section treats the moments of  $\alpha_1$  and  $\alpha_2$  separately. Only in the last step are the global properties embodied in  $M_q^{(1)}$  and

$M_q^{(2)}$  related through the exponent  $\eta$  in Eq.(10). In that approach the pairing of  $\alpha_1$  with  $\alpha_2$  in each channel is not taken into account. However, we know that there are channels, such as Ch. 1 in Figs. 1 and 2, where the absence of a dominant mode of oscillation results in  $\alpha_1 \approx \alpha_2$ . Thus the correlation between the two scaling exponents is an important feature that should be explored and quantified. To that end we define

$$\beta = \alpha_2/\alpha_1 \quad (12)$$

for each channel. In most cases we have  $\beta < 1$ , but  $\beta > 1$  is possible and, by its rarity, noteworthy.

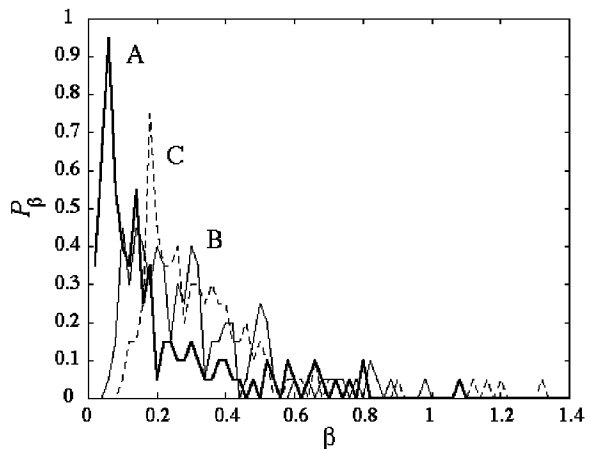


FIG. 8. The distributions of the  $\beta$  values of the subjects A, B, and C.

From a scatter plot, such as Fig. 3, it is possible to visualize the  $\beta$  distribution, since  $\beta$  is just the slope of a line from the origin to each point. We show in Fig. 8 the  $\beta$  distributions for the same three subjects as those in Fig. 7. Subject B is chosen for display because it has the largest  $\eta$ , while subject C is chosen because it has several  $\beta$  values that exceed 1.

To summarize the 128 values of  $\beta_j$  for each subject, we apply to them the moment analysis that is developed in Sec. 4. Let us therefore define

$$N_q = \frac{1}{N} \sum_{j=1}^N \beta_j^q / \left( \frac{1}{N} \sum_{j=1}^N \beta_j \right)^q. \quad (13)$$

The  $q$  dependence of  $\ln N_q$  for the same three subjects are shown in Fig. 9. Again, linear fits are very good. Thus we have

$$N_q \propto \exp(\nu q) \quad (14)$$

with a distinct  $\nu$  for each subject. Clearly, the ones with wide  $\beta$  distributions relative to their means have higher values of  $\nu$ .

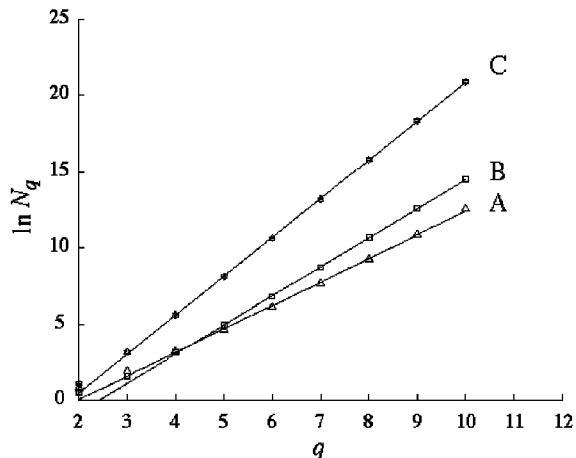


FIG. 9. The  $q$  dependence of  $\ln N_q$  for subjects A, B, and C.

## VI. SEPARATING STROKE FROM NORMAL SUBJECTS

Up to this point we have deliberately chosen not to discuss the conditions of the subjects so that attention could be focused on the method of analysis and the existence of scaling behavior in EEG generally. Now we state that among the 28 subjects, eighteen are normal and ten have acute ischemic stroke. Both subject groups exhibit these scaling behaviors. We have analyzed their EEG time series in identical ways and determined the two indices,

$\eta$  and  $\nu$ , for each subject. Figure 10 shows a scatter plot of  $(\eta, \nu)$  for all 28 subjects. The normal subjects are labeled by open circles and the stroke subjects by filled circles. The values of  $(\eta, \nu)$  are widely distributed for the 28 subjects, and with one exception the two subject groups are distinctly separated. The normal subjects are all restricted to a narrow wedge region in the  $(\eta, \nu)$  plot. The stroke subjects are scattered over a large area outside the wedge. There is one stroke subject whose  $\eta$ - $\nu$  values lie inside the wedge for reasons that are not yet understood. Nevertheless, in this initial attempt to categorize the subjects we have achieved 100% success rate in finding the normal subjects confined to the wedge region, and 90% rate in finding the stroke subjects outside it. To our knowledge, the conventional approach to stroke detection with EEG, using Fourier power spectrum analysis combined with topographic plotting, does not have such a high rate of success in discriminating the subjects [11,14].

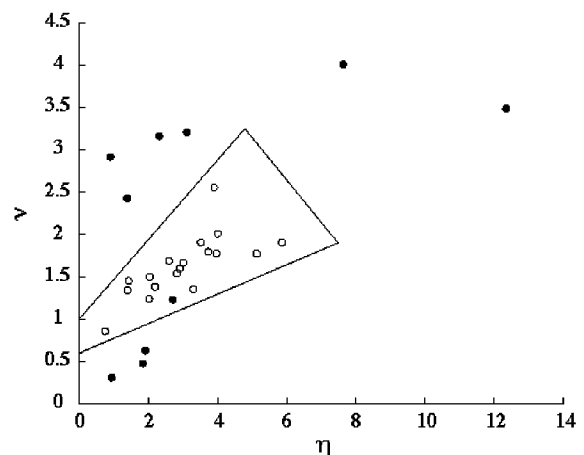


FIG. 10. Scatter plot of  $\nu$  versus  $\eta$  for all 28 subjects. Open circles indicate 18 normal subjects. Closed circles indicate 10 subjects with acute ischemic stroke. The significance of the wedge region is discussed in the text.

It is outside the scope of this paper to examine further the clinical conditions of the subjects to pur-

sue an understanding of the one exception. We emphasize instead that, based upon these results, the approach seems very promising. To be sure, more subjects in both groups must be studied to confirm the utility of this approach as a clinical discriminator of stroke. It is likely that the measures developed here will find wider utility when applied to diverse data sets and subject conditions. Our objective in this paper is mainly to describe the method that gives rise to an interesting and useful result. We believe that the existence of scaling behavior in  $F(k)$  as computed here, and its apparent success in this clinical application, are sufficient to justify *a posteriori* our unconventional application of DFA to continuous EEG time series.

## VII. CONCLUSION

Recognizing that the brain is a highly complex system, we have explored a way of analyzing the EEG time series that avoids the assumptions of linearity and low-dimensional chaos. By studying the fluctuations from linear trends defined over varying time scale, we have found two scaling regions in which the RMS fluctuations can be characterized by two dimensionless scaling exponents,  $\alpha_1$  and  $\alpha_2$ , for each channel. We then performed moment analyses to reduce the large number of pairs of  $(\alpha_1, \alpha_2)$  to simple summary statistics. The two types of independent moments,  $M_q^{(i)}$  and  $N_q$ , yield two indices,  $\eta$  and  $\nu$ , which provide concise signatures of the nonlinear behavior of all channels of the EEG signals.

Our emphasis in this paper has been on the method of analysis more than on the clinical study of the subjects. Nevertheless, working with 28 subjects is sufficient to demonstrate the effectiveness of the method, to show the universality of the scaling behaviors, to reveal the range of variability of the

indices derived, and to offer the possibility of a new way of thinking about global human brain dynamics. The initial indication that our analysis can lead to categorization of the subjects according to their locations in the  $(\eta, \nu)$  plot offers realistic hope that the method proposed has possibilities of becoming an effective diagnostic tool.

## Acknowledgments

We are grateful to Prof. Don Tucker and Dr. Phan Luu of EGI for supplying the EEG data for our analysis. We have also benefited from the computational assistance of Wei He. This work was supported, in part, by the U. S. Department of Energy under Grant No. DE-FG03-96ER40972, and the National Institutes of Health under Grant No. R44-NS-38829.

- 
- [1] *Electroencephalography: Basic Principles, Clinical Applications, and Related Fields*, edited by E. Niedermeyer and F. H. Lopes da Silva (Urban and Schwarzenberg, Baltimore, 1987); *ibid* (Williams and Wilkins, Baltimore, 1998).
  - [2] P. L. Nunez, *Neocortical Dynamics and Human EEG Rhythms* (Oxford University Press, 1995).
  - [3] S. Blanco, C. D'Attellis, S. Isaacson, O. A. Rosso, and R. Sirne, *Phys. Rev. E* **54**, 6661 (1996); S. Blanco, A. Figliola, R. Quian Quiroga, O. A. Rosso, and E. Serrano, *Phys. Rev. E* **57**, 932 (1998).
  - [4] *Chaos in Brain?*, edited by K. Lehnertz, J. Arnhold, P. Grassberger and C. E. Elger (World Scientific, Singapore, 2000).
  - [5] B. H. Jansen and M. E. Brandt, *Nonlinear Dynamical Analysis of the EEG* (World Scientific, Singapore, 1993).

- [6] K. Lehnertz and C. E. Elger, Phys. Rev. Lett. **80**, 5019 (1998).
- [7] C.-K. Peng, S. V. Buldyrev, S. Havlin, M. Simons, H. E. Stanley, and A. L. Goldberger, Phys. Rev. E **49**, 1685 (1994).
- [8] C.-K. Peng, S. Havlin, H. E. Stanley, and A. L. Goldberger, Chaos **5**, 82 (1995).
- [9] Watters, P. A. Complexity International **5**, 1 (1998).
- [10] P. Luu and D. Tucker (private communication).
- [11] Nagata, K. (1988). Brain Topography **1**(2), 97-106.
- [12] C. W. Gardiner, *Handbook of Stochastic Methods* (Springer-Verlag, Berlin, 1983).
- [13] R. C. Hwa, Phys. Rev. D **41**, 1456 (1990).
- [14] Luu, P., D. M. Tucker, R. Englander, A. Lockfield, H. Lutsep, and B. Oken (2001). Journal of Clinical Neurophysiology **18**, 302-317.